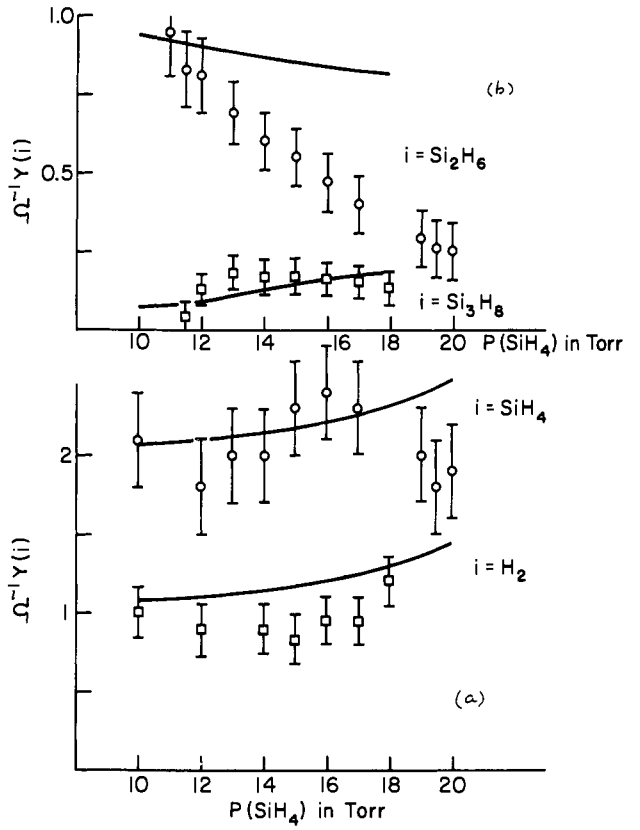

Figure 7. Comparison of calculated normalized yields with experimental values. (a) O, SiH_4 decomposition; □, H_2 formation. (b) O, Si_2H_6 formation; □, Si_3H_8 formation. Fluence = 1.0 J/cm^2.

(2) SiH_2 and SiH_3SiH are taken to be at the same *vibrational* temperature as SiH_4 and classical vibrational heat capacities are assumed.

(3) Vibrational frequencies for the Si_2H_6 and Si_3H_8 molecules were taken from the literature.[24,40] The reaction coordinates for (5) and (10) were taken to be Si-H stretching modes while that for (9) was assumed to be a Si-Si stretching mode; the corresponding frequencies were simply removed for the respective transition states of the unimolecular decompositions, (5), (9) and (10).

(4) The collisional stabilization rate constants, k_6 and k_{11}, were taken to be 1.7×10^{-11} cm^3/s as reported from experimental studies of the collisional stabilization of UF_6.[41]

The results of the calculations are shown by the solid lines in Figure 7, while the points shown are the experimental values. Considering the crudeness of the calculations, the agreement with experiment must be considered as satisfactory.

The much more rapid decrease in the observed normalized yield of Si_2H_6, as compared with the calculated yield, is probably due to the occurrence of secondary reactions that destroy the very reactive Si_2H_6.[23] A corresponding destruction of Si_3H_8 would also be expected and while the data seem in accord, it is not as evident as in Si_2H_6 due to the much lower concentration.

4. Effect of He on the Formation of Si_2H_6 and Si_3H_8. The data in Figure 1 show that within experimental error, He is just as effective in promoting absorption of laser energy as is SiH_4. However, the results in Figure 4 show that He is not as effective as SiH_4 in increasing the formation of Si_3H_6 but is more effective than SiH_4 in increasing the formation of Si_3H_8. This is probably to be understood on the basis that He is a less effective third body for the stabilization of Si_2H_6* in reaction 6 than is SiH_4. The data in Figure 4 suggest, and it is born out by experiment, that the rate of reaction of SiH_4 depends only on total pressure for P(SiH_4) ≥ 15 torr and, therefore, in view of Figure 1, only on the average number of quanta per molecule.

The addition of He clearly increases the rate of reaction, as shown in Figure 4, and therefore the infrared laser induced decomposition of SiH_4 is a pressure-dependent multiphoton photodecomposition and not a thermal reaction. The success of the treatment employed here indicates that for multiphoton processes in which collisions are necessary to reach the quasicontinuum and in which reaction occurs with $\bar{v}$ in the range of 2-4, one may assume that the vibrational energy from the laser radiation may be taken to be in a nondegenerate Boltzmann distribution characterized by the average number of quanta absorbed per molecule.

Acknowledgment. This work was supported by the U.S. Department of Energy under Contract No. DE-ASO2-76ERO3416.

(40) T. L. Pollock, H. S. Sandhu, A. Jodhan, and O. P. Strausz, *J. Am. Chem. Soc.*, **95**, 1017 (1973).

(41) H. E. Bass, F. D. Shields, W. D. Breshears, and L. B. Asprey, *J. Chem. Phys.*, **67**, 1136 (1977).

Induced Optical Activity and Liquid Crystal Linear Dichroism of 9,9′-Spirobi[9*H*-fluorene]

P. Palmieri[1a] and B. Samorì*[1b]

Contribution from Istituto di Chimica Fisica e Spettroscopia and Istituto di Chimica degli Intermedi, Facolta' di Chimica Industriale, 40136 Bologna, Italy. *Received December 15, 1980*

Abstract: A direct confirmation of the mechanism of induction of optical activity proposed by Craig and Stiles for molecules of D_{2d} or S_4 symmetry, on the basis of Jahn-Teller distortion of degenerate excited states producing excited enantiomeric species discriminated in energy in a chiral environment, has been sought by direct measurement of the induced circular dichroism of the spirobifluorene molecule. The shape of the measured induced circular dichroism for the lowest transition in *d*- and *l*-diethyl tartrate is consistent with the Craig-Stiles model, even though other mechanisms of induction of optical activity appear to be active and contribute to the CD signal of this molecule in chiral solvents.

An achiral molecule, dissolved in a chiral solvent, becomes chiral and displays induced circular dichroism (ICD). ICD has been recorded for several molecules in different environments,[2] and theoretical models have been proposed[3-5] to show that ICD may

0002-7863/81/1503-6818$01.25/0

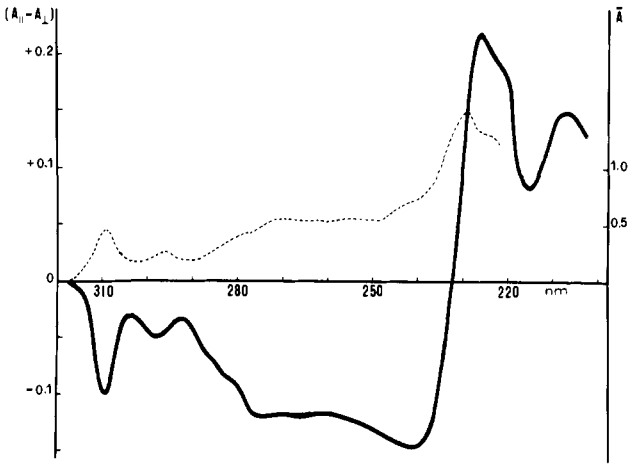

Figure 1. LCLD spectrum (—) and the absorbance (A) measured with unpolarized light (---) of an oriented sample of SBF dissolved in a cyclohexylcyclohexane nematic mixture.

arise from the electric multipole moments of the chiral solvent molecules, which mix the states of the achiral solute molecules, and from the dispersive interactions due to the dynamic coupling of the electronic states of the solute and solvent molecules. In addition, the local polarization fields inside a chiral medium can make unequal contributions to the amplitude of the left and right circularly polarized radiations initially equal at incidence.[4] Such "macroscopic ICD" is proportional to the circular birefringence of the solution and is not dependent on the anisotropic physical properties of the solute.

More recently Craig and Stiles[6,7] have proposed an additional mechanism for ICD of electronic transitions to degenerate electronic states in molecules belonging to the D_{2d} or S_4 symmetry group.

According to the latter mechanism, Jahn–Teller vibronic interaction discriminates between the equilibrium geometries of the solute molecules in the doubly degenerate states producing two enantiomeric species which are separated in energy by intermolecular effects.

To our knowledge, no experimental ICD of molecules capable of exhibiting the Jahn–Teller effect has been reported. We have measured the circular dichroism of 9,9'-spirobi[9*H*-fluorene] (SBF) dissolved in chiral solvents and confirmed the assignment of the UV spectrum of this molecule[8] by linear dichroism measurements and theoretical computations.

Results and Discussion

Liquid Crystal Linear Dichroism (LCLD) of SBF. The Jahn–Teller mechanism of induction of optical activity for SBF becomes active only when the excited state has E symmetry. The available interpretation of the UV absorptions of this molecule relies on the LD measurements of Sagiv et al.,[8] which have been obtained by a static method using stretched polymeric films. Since criticisms have been raised[9] about some quantitative aspects of the analysis of LD measurements in ref 8, we have measured the LD of SBF using a liquid crystal solvent and a more sensitive modulation technique[10] which allows the difference of the two absorbances ($A_{\parallel} - A_{\perp}$) to be recorded directly.

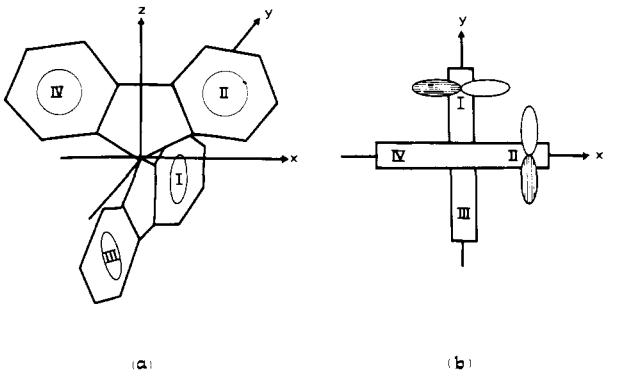

Figure 2. Reference system for (a) spiro compounds and SBF and (b) spiro interactions. Numbering of the benzenic subunits in SBF.

The profile of the LD spectrum in Figure 1 shows differences when compared to the LD spectrum in Figure 9 of ref 8, but this does not affect the assignments of the lowest UV absorptions. It is assumed that SBF is oriented in the liquid crystal matrix as in stretched polyethylene films.[8] The negative linear dichroism ($A_{\parallel} - A_{\perp}$), which dominates the lowest energy region up to 240 nm, is assigned to the $E \leftarrow {}^1A_1$ transitions and the positive LD at higher energy to the ${}^1B_2 \leftarrow {}^1A_1$ transitions.

The band shapes of the LCLD and isotropic spectra do not provide evidence of steric distortions of the D_{2d} symmetry due to the "liquid crystal field".[11]

Excited States of SBF and Assignment of the UV and LD Spectrum. To obtain the theoretical expressions of the π–π^* excited state wave functions of spiro compounds by using the Hückel method or other semiempirical treatments restricted to π electrons, two approaches have been used. In the first, the π orbitals of the two cyclic unsaturated subunits, which constitute the molecule (Figure 2), have been considered as noninteracting. This leads to MO's which are localized over either of the two units. The excited states of the two component fragments interact by dipole–dipole interactions, leading to exciton-like wave functions for the excited states of these molecules.[8]

In the second treatment, the so called spiro interactions among the π atomic orbitals (Figure 2) are taken into account, leading to MO's which are delocalized over the entire molecule.

As shown by Simmons et al.,[12] delocalization gives important contributions to the theoretical values of the spectral properties such as transition energies and intensities. Accordingly, we have included in the one electron PPP Hamiltonian the spiro interaction matrix elements which have been assumed proportional to the corresponding overlap integrals. Transition energies and oscillator strengths have been evaluated by the two CI treatments described in ref 7. A limited CI was followed by a more extended CI treatment, where all single and double excitations from selected reference configurations have been included.

The PPP parametrization and CI method used for these computations reproduce closely the transition energies and oscillator and rotational strengths computed for a simpler spiro compound (spiro[4.4]nonatetraene) by ab initio methods.[7]

The approximate expressions of the MO's of SBF of the various symmetry species are given by the general expressions

$$b_2(\pi) = \pi_1 + \pi_{II} + \pi_{III} + \pi_{IV}$$

$$b_3(\pi) = \pi_1 - \pi_{II} + \pi_{III} - \pi_{IV}$$

$$a(\pi) = \pi_1 + \pi_{II} - \pi_{III} - \pi_{IV}$$

$$b_1(\pi) = \pi_1 - \pi_{II} - \pi_{III} + \pi_{IV}$$

where π is a bonding or an antibonding molecular orbital of the four benzenic subunits (I–IV) in the molecule. By denoting as 1, 2, and 2' the π-bonding benzene MO's and 1*, 2*, and 2'*, the

(1) (a) Istituto di Chimica Fisica. (b) Istituto degli Intermedi.
(2) Tajiri A.; Hirayma H.; Hatano M. *Chem. Phys. Lett.* **1980**, *70*, 22–26 and references therein.
(3) Craig, D. P.; Power, E. A.; Thirunamachandran, T. *Chem. Phys. Lett.* **1974**, *27*, 149–153.
(4) Mason S. F. *Chem. Phys. Lett.* **1975**, *32*, 201–203.
(5) Schipper, P. E. *Mol. Phys.* **1975**, *29*, 1705–1716.
(6) Craig, D. P.; Stiles, P. J. *Chem. Phys. Lett.* **1976**, *41*, 225–227.
(7) Craig, D. P.; Stiles, P. J.; Palmieri, P.; Zauli C. *J. Chem. Soc. Faraday Trans. 2* **1979**, *75*, 97–104.
(8) Sagiv, J.; Yogev, A.; Mazur Y. *J. Am. Chem. Soc.* **1977**, *99*, 6861–6869.
(9) Thulstrup, E. W.; Michl, J. *J. Phys. Chem.* **1980**, *84*, 82–93.
(10) Samorì, B.; Mariani, P.; Spada, G. P. *J. Chem. Soc., Perkin Trans. 2*, in press.
(11) Samorì, B. *J. Phys. Chem.* **1979**, *83*, 375–378.
(12) Simmons, H. E.; Fukunaga, T. *J. Am. Chem. Soc.* **1967**, *89*, 5208–5220. Batich, C.; Heilbronner, E.; Rommel, E.; Semmelhac, M. F.; Foos, J. S. *J. Am. Chem. Soc.* **1974**, 7662–7668.

Table I. Configuration Interaction π Energies (cm^{-1}) and Eigenfunctions for the Ground and First Few Excited States of SBF[a]

state	symmetry	f value of transition		leading terms in the CI wave functions	energy, cm^{-1}	
		limited CI	extended CI		limited CI	extended CI
D_{2d}	D_2					
A_1	A			ground-state config	0	0
B_2	B_1	0.0020	0.0042	0.53[12,15] + 0.40[11,18] -0.43{[9,13] + [8,14]}	38020	40742
B_1	A	0	0	0.45[12,18] + 0.46[11,15] -0.45{[9,14] + [8,13]}	38152	38415
E	B_3	0.0057	0.0058	0.44[12,16] + 0.41[11,17] -0.43[10,13] - 0.39[7,14]	38700	39184
E	B_2	0.0057	0.0058	0.44[12,17] + 0.41[11,16] -0.43[10,14] - 0.39[7,13]	38700	39184
E	B_2	0.2338	0.3446	0.74[12,14] + 0.56[11,13]	40918	41028
E	B_3	0.2338	0.3446	0.74[12,13] + 0.56[11,14]	40918	41028
E	B_2	0.2000		-0.54[12,17] + 0.58[11,13] -0.46[10,14]	49238	
E	B_3	0.2000		-0.54[12,16] + 0.58[11,14] -0.46[10,13]	49238	
B_2	B_1	0.7849		0.45[12,15] + 0.43[10,15] + 0.36{[9,16] + [8,17]}	49062	

[a] The MO indexes follow the computed energy sequence of the occupied and unoccupied orbitals. Oscillator strengths (f) of the electronic transition.

Table II. Effect of the I-IV[a] Permutation Inversion Symmetry Operation on the Electronic (q, p) and Nuclear (Q, P) Coordinates and Momenta and on the Electronic $T(\mathbf{p})$, $V(\mathbf{q},Q)$ and Nuclear $T(P)$, $E_{B_n}(Q)$ Potential Energy Operators[a]

E	$\mathbf{q} = x, y, z$	Q	$\mathbf{p} = p_x, p_y, p_z$	$T(\mathbf{p})$	$V(\mathbf{q},Q)$	P
I-IV[a]	$\mathbf{q}' = -y, x, -z$	$-Q$	$\mathbf{p}' = -p_x, p_y, -p_z$	$T(\mathbf{p}') = T(\mathbf{p})$	$V(\mathbf{q}',-Q) = V(\mathbf{q},Q)$	$-P$
E	$T(P)$	$B_2(Q)$	$B_3(Q)$	$E_{B_3}(Q)$		
I-IV[a]	$T(P)$	$-B_3(-Q)$	$B_2(-Q)$	$E_{B_2}(-Q)$		

[a] By I-IV we denote a cumulative permutation of the atomic nuclei of the benzene units in SBF. E is the identity operation.

corresponding π^* antibonding MO's, the energy sequence of the occupied orbitals of SBF is found to be $b_2(1)$, $b_3(1)$, $a(1)$, $b_1(1)$, $b_3(2)$, $b_2(2)$, $a(2')$, $b_2(2')$, $b_3(2')$, $b_1(2')$, $a(2)$, $b_1(2)$ while the orbital sequence in the virtual subspace is $b_2(2^*)$, $b_3(2^*)$, $a(2'^*)$; $b_2(2'^*)$, $b_3(2'^*)$, $b_1(2'^*)$, $a(2^*)$, $b_1(2^*)$, $b_2(1^*)$, $b_3(1^*)$, $a(1^*)$, $b_1(1^*)$. The excited state wave functions and the transition properties computed for SBF are listed in Table I. The four lowest states of SBF are related to the L_b-benzenoid state. Out of the possible linear combinations of the L_b-benzenoid states, two of the combinations correspond to allowed degenerate transitions x, y polarized and one to a z polarized transition. The energy ordering of these two levels is inverted on passing from the restricted to the extended CI description. The measured dichroic ratios indicate x, y polarization for the lowest transition (310 nm) in agreement with the present computations and a previous assignment.[8] Compared to the first absorption, the next two absorptions (270 and 240 nm) have identical dichroic ratios and are assigned to the next two excited states of E symmetry.

According to Sagiv,[8] these states have a pure benzenic L_a or B character, but the wave functions in Table I suggest mixed L_a and B character for these states. The corresponding state with B_2 symmetry, has a z polarized transition moment. The intense absorption at 200 nm with positive linear dichroic ratio is assigned to this state.

Optical Activity of SBF Induced by the Jahn–Teller Effect. By the Jahn–Teller theorem, the SBF molecule is not stable at the D_{2d} geometry in the excited states of E symmetry. Stabilization of these states may occur for displacements along the internal coordinate[13]

$$Q = -\delta x_1 - \delta y_{II} + \delta x_{III} + \delta y_{IV} \qquad (1)$$

leading to excited D_2 chiral structures, where the degenerate E levels are split into B_2 and B_3 components. Given the reference system in Figure 2 and the numbering of the benzene units, positive values of the Q coordinate correspond to P helicity (Figure 3) and negative values to M helicity.

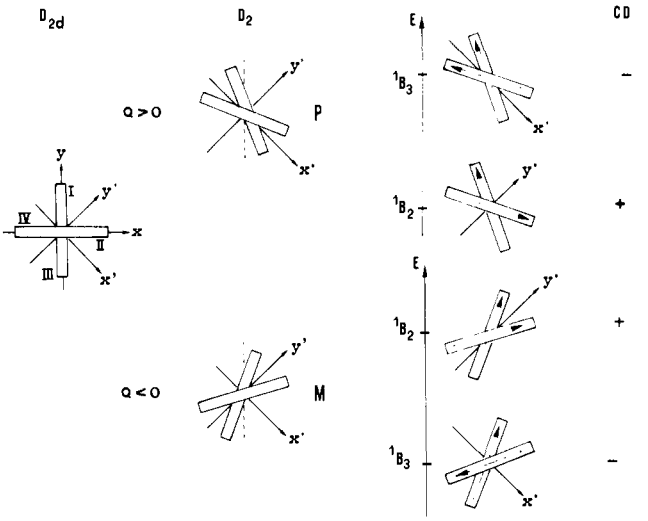

Figure 3. M and P chiral structures of twisted SBF. Relative ordering of the B_2 and B_3 components of the E states for the two chiral structures and the sign of the CD of the corresponding electronic transitions; x and y are the reference axes for the undistorted D_{2d} geometry and x' and y' are the symmetry axes for the distorted D_2 geometries.

By using the transformation properties of the electronic and nuclear coordinates ($\mathbf{q}$, Q) and momenta ($\mathbf{p}$, P), of the electronic $T(\mathbf{p})$, $V(\mathbf{q},Q)$, and nuclear $T(P)$ and $E(Q)$ kinetic and potential energy operators under the permutation inversion symmetry operations of the molecular symmetry group,[14] the adiabatic potential curve for the B_2 state

$$\{T(\mathbf{p}) + V(\mathbf{q},Q)\}B_2(\mathbf{q},Q) = E_{B_2}(Q)B_2(\mathbf{q},Q) \qquad (2)$$

is related to the B_3 potential energy curve

$$\{T(\mathbf{p}') + V(\mathbf{q}',-Q)\}B_3(\mathbf{q}',-Q) = E_{B_3}(-Q)B_3(\mathbf{q}',-Q)$$

$$E_{B_2}(Q) = E_{B_3}(-Q) \qquad (3)$$

(13) δx_1, δy_{II}, . . . are cumulative nuclear displacements for atoms of the benzene rings I, II, . . ., respectively, following the numbering given in Figure 3.

(14) For general reference, see: Bunker, P. R. In "Molecular Symmetry and Spectroscopy"; Academic Press: New York, Chapters 2 and 9.

(15) Cremaschi P. *Mol. Phys.*, in press.

Table III. Rotatory Strengths[a] for the Lowest $^1E \leftarrow {}^1A_1$ Transition in Spiro[4.4]nonatetraene and SBF of D_{2d} Geometry Computed with the Extended PPP CI Method. Comparison with the Ab Initio Values[b]

		spiro[4.4]nonatetraene		SBF	
transition	state	dipole length	dipole velocity	dipole length	dipole velocity
$^2E \leftarrow {}^1A_1$	B_2	257 (76)	189 (26)	18	30
	B_3	−257 (−76)	−189 (−26)	−18	−30

[a] 10^{-40} cgs units. [b] Ab initio values in parentheses.

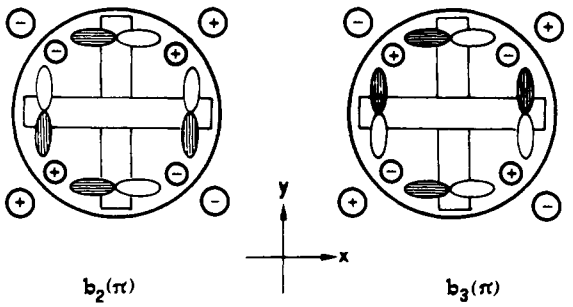

Figure 4. Quadrupole–quadrupole solute–solvent interaction: one electron interactions for MO's of b_2 and b_3 symmetry. Quadrupole components of the b_2 and b_3 charge distributions (inner sphere and quadrupole components of the solvent potential (outer sphere).

Using the symmetry relationships in Table II, it is also shown that the vibronic wave functions for the two states $\beta_n(Q)$ $B_n(\mathbf{q},Q)$ (n = 2, 3) are not coupled by the nuclear momentum operator P, thus leading to uncoupled and symmetry related vibronic wave functions for the two states.

$$\{T(P) + E_{B_n}(Q)\}\beta_n(Q) = \epsilon\beta_n(Q) \quad (n = 2,3) \qquad (4)$$

Hence the SBF molecule in each excited state of E symmetry behaves as a racemic mixture of two degenerate conformational enantiomers. The chirality of the D_2 structures can be easily predicted by qualitative arguments based on molecular orbital or exciton theories: a M chiral configuration is expected to display at lowest energy a negative CD band corresponding to the B_3 component (Figure 3) while B_2 is the lowest excited state in the P isomer corresponding to positive CD.

This agrees with the results of actual computations on -spiro-[4.4]nonatetraene and SBF as shown in Table III. The interaction with a chiral environment, by stabilizing one of the two enantiomeric forms, allows instrumental recording of their circular dichroism.

The possibility of an experimental observation of the Jahn–Teller ICD depends upon the shape of the potential functions of the two degenerate excited states and upon the nature of the solvent which provides the discrimination energy between the P and the M geometry.

Since the quadrupole is the lowest nonzero multipole component of the charge density of the B_2 and B_3 states, the simplest conceivable source of chiral discrimination is provided by the quadrupole component of the electrostatic potential due to the solvent molecules. For example, the b_3 MO is seen to be stabilized and the b_2 MO destabilized in the quadrupole field represented in Figure 4.

By neglecting the Q dependence of the molecular wave functions (crude adiabatic approximation), this interaction shifts by a constant in the opposite directions, the two potential energy curves and the vibronic eigenvalues (eq 4), for the two electronic states. The resulting potential energy curves are shown in Figure 5b and 5c where the vibronic structures of ICD are also reported. The vibronic intensities have been obtained by multiplying the rotational strengths in Table III by the appropriate Boltzmann and Franck–Condon factors which have been evaluated by solving the vibronic eigenfunctions (eq 4), using the potential energy curves computed in ref 7 and the method of ref 15, assuming an energy discrimination between the two chiral forms of ±500 cm^{-1}. The latter values are in the range of chiral discriminating energies[16] and are compatible with the measured splitting of the lowest transition of SBF, derived from the CD spectrum (see Figure 6) of the molecule.

The 0–0 vibronic band of the lowest energy component of the ICD couplet (Figure 5b,c) is red shifted and less broad compared to the isotropic absorption (Figure 5a). Its sign may be negative or positive depending on the relative stability of the P and M enantiomeric forms in the chiral medium.

After the first band, overlapping and partial cancellation of the vibronic bands of the two components of the couplet are expected to occur, with partial cancellation of the quasi-sigmoidal shape of the lowest vibronic components of the ICD (see Figure 5b,c). Given the LD spectrum in Figure 1, further cancellation effects could originate from vibronic interactions with other excited states and from other mechanisms of induction of CD.

Experimental Measurements of ICD of Fluorene and SBF. After an unsuccessful attempt of including SBF in the chiral hydrophobic cavities of β-cyclodextrin molecule,[17] an ICD spectrum has been observed by dissolving SBF in an aqueous micellar solution of sodium deoxycholate [18](DcNa). The DcNa micellar aggregates are capable of including hydrophobic reactants into their chiral interior inducing optical activity.[19]

The ICD signals are all positive and clearly different from zero for the first band at 309 nm and also for the region between 285 and 250 nm. At the shortest wavelength the CD spectrum is dominated by the absorption of DcNa (Figure 6).

The small red shift (~0.6 nm) of the lowest energy CD band with respect to the isotropic absorption suggests the presence of two CD bands with opposite signs and the splitting of the lowest electronic transition of SBF. The presence of a doubly signed CD couplet is clearly seen in a solution of *l*-diethyl tartrate (Figure 6). It was verified that (i) the CD signals reverse their signs passing from solutions of *l*-diethyl tartrate to solutions of *d*-diethyl tartrate, (ii) the CD absorption intensities are proportional to the concentration of SBF, (iii) the CD absorption intensities are temperature dependent, increasing by ~80% when the temperature is lowered from 25 to 45 °C (at this temperature the diethyl tartrate solution crackles).

By changing the solvent or the spectral region other mechanisms of induction of CD become important. In particular, an electronic transition of the solute molecule borrows chirality from one or more electronic transitions of the solvent by the dynamic coupling mechanism.[4,5] ICD has, in this case, the same sign of the inducing transition, being proportional to the dipole and rotational strengths of the coupled transition and inversely proportional to the square of the energy difference between the solvent and solute transition energies.[4,5] In fact, in *d*-2-phenylbutanoic acid, which has an intense absorption edge close to the lowest energy SBF band, the doubly signed ICD of SBF disappears, and the ICD and the isotropic absorptions have similar spectral profiles (Figure 7).

Since SBF consists of two fluorene subunits, the UV spectrum of fluorene is very similar to the UV spectrum of SBF.[8] Moreover fluorene, belonging to the C_{2v} symmetry group has no degenerate excited states and cannot exhibit the Jahn–Teller splitting. For these reasons, we have attempted to record the ICD of fluorene

(16) Craig, D. P. In "Optical Activity and Chiral Discrimination"; Mason S. F., Ed.; D. Reidel: Dodrecht, Holland, 1979. Mason, S. F. *Ibid.*; D. Reidel: Dodrecht, Holland, 1979.
(17) Shimizu, H.; Kaito, A.; Hatano, M. *Bull. Chem. Soc. Jpn.* **1979**, *52*, 2678–2684.
(18) Nair, P. P.; Kritchevsky, D. "The Bile Acids"; Plenum Press: New York, 1971, Vol. 1, Chapter 8.
(19) Gawronski, J. *Tetrahedron Lett.* **1976**, *42*, 3845–3846.

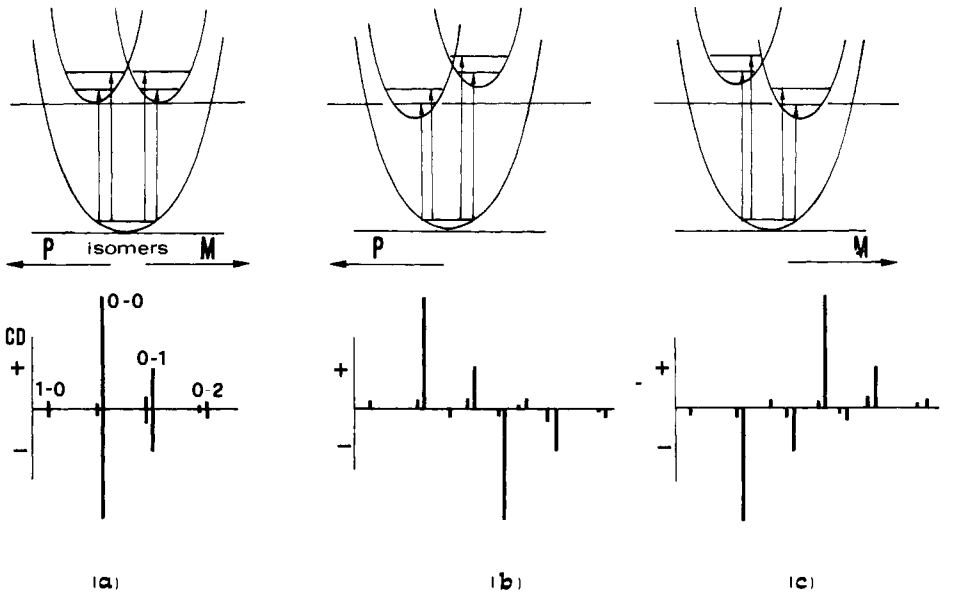

Figure 5. Adiabatic potential curves for the B_2 and B_3 states in SBF in (a) isotropic and (b),(c) anisotropic media. Vibronic structure of the CD for the two electronic transitions. Franck–Condon and Boltzman factors have been evaluated from the ab initio potential curves in ref 7 and the discrimination energies of the two chiral forms ($M - P$) taken ± 500 cm^{-1} in Figure 6a, and 6b, respectively.

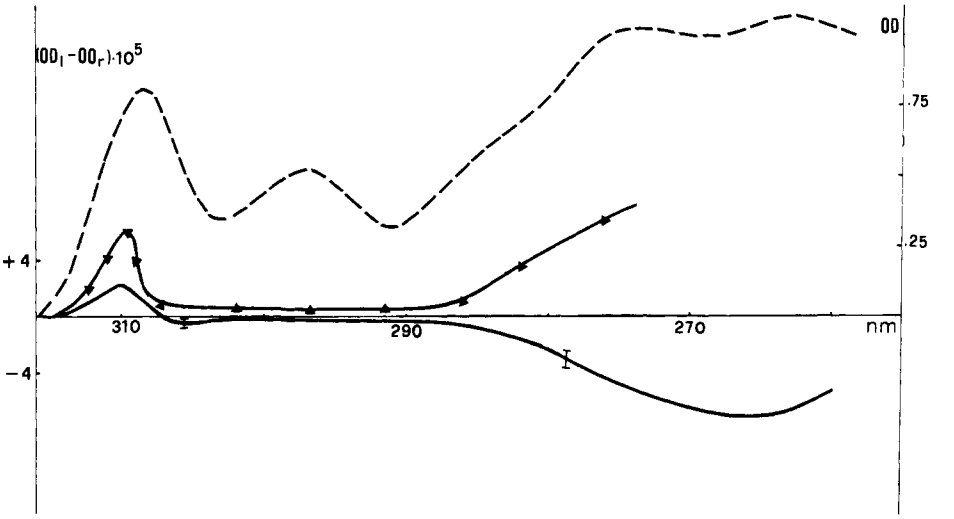

Figure 6. Measured ICD of SBF in *l*-diethyl tartrate (—) and DcNa (▲). Isotropic absorption (---).

in solutions of *l*- and *d*-diethyl tartrate. At the sensitivity of our instrumentation, the ICD signal of fluorene is nearly undetectable. A small signal corresponding to the lowest transition was recorded. Its intensity is one order of magnitude lower than the ICD of SBF, the *g* factor for the latter molecule being $\simeq 3 \times 10^{-5}$.

By contrast, the intensity of the spectrum of fluorene in *d*-2-phenylbutanoic acid is higher than the ICD of SBF, proving that the dispersion mechanism provides, in this case, the dominant contribution to the ICD spectra of SBF and fluorene in the 300-nm region (Figure 7).

It is concluded that the Jahn–Teller contribution to the ICD of SBF in solution of *d*- and *l*-diethyl tartrate is observed due to the low efficiency of the solvent in inducing CD by the dispersion mechanism in the lowest absorption region of SBF.

Conclusions

The ICD of the lowest $^1E \leftarrow {}^1A_1$ transition of SBF in *d*- and *l*-diethyl tartrate is consistent with the Jahn–Teller scheme proposed by Craig and Stiles. The potential energy curves in Figure 5 and the values of the rotatory strengths in Table IV suggest a preferential stabilization of the *P* enantiomeric form in *l*-diethyl tartrate and DcNa.

The ICD at higher energies orginates from excited states of identical *E* symmetry and has opposite sign in DcNa and *l*-diethyl tartrate. This could be due either to a different energy pattern

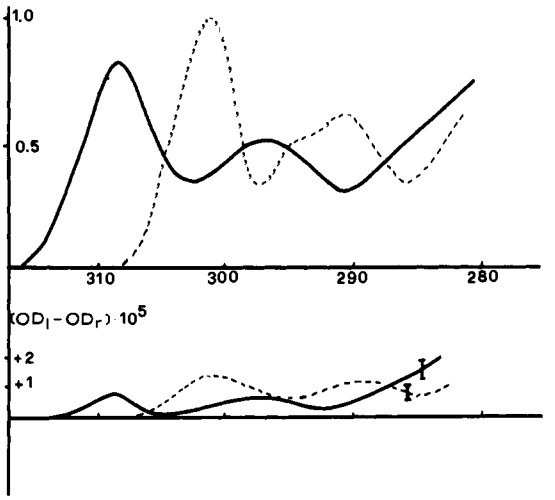

Figure 7. Isotropic absorption (upper) and ICD spectra (lower) of SBF (full line) and fluorene (dashed line) in *d*-2-phenylbutanoic acid.

for the two components of the E level in the two solvents or to dispersion ICD which is expected, on energy ground, to be at least

three times larger for the transitions at 265 nm compared to the transition at 310 nm.

The low circular birefringence of the solvents used for the present investigations rules out the possibility of relevant contributions to ICD of "macroscopic mechanism".

The presence of more than one mechanism for the induction of the optical activity prevents any quantitative analysis of the intensity of ICD signals to obtain information on the geometries and chiral discrimination energies for the two enantiomeric excited species originated by the Jahn-Teller mechanism.

The circular dichroism of the fluorescence of SBF, dissolved in a chiral solvent, which should be dominated by the more stable of the two chiral species is likely to provide more conclusive experimental evidence for the Jahn-Teller mechanism of induction of circular dichroism.

Experimental Section

The CD spectra have been recorded by a Jouan II and a JASCO J 500 dichrograph/DP 500 data processor. The *l*- and *d*-diethyl tartrates, which have been synthetized by the procedure described in ref 20, have $[\alpha]_D$ -7.3 and +6.5° respectively, and the *d*-2-phenylbutanoic acid[21] has $[\alpha]_D$ +102°.

The concentration of DcNa was 0.19 M, well above the critical micellar concentration, in phosphate buffer at pH 7.8. In all cases, the base line of the ICD spectra was obtained by recording the CD spectra of the pure chiral solvent or of solutions of SBF or fluorene in racemic solvents with solute concentrations identical with those used for the ICD measurements. The LCLD spectra have been recorded by the JASCO/LD attachment using a nematic liquid crystal matrix trasparent to the UV radiation (E. Merck—ZLI 1167) oriented by surface coupling agents.[10]

Acknowledgment. We are grateful to Professor Prelog (Zürich) for supplying a sample of SBF which has made possible this work. We acknowledge correspondence with Professor D. P. Craig (Camberra) and Dr. P. Stiles (North Ryde, Australia) on the subject of ICD, and we are grateful for their helpful suggestions. We are grateful to Professor A. D. Buckingham (Cambridge) for a useful discussion at the symposium held in Florence (1980) on "Solute-Solute, Solute-Solvent Interactions", where part of this work has been presented. E. Merck (Darmstadt) and Dr. P. Biscarini (Bologna) have provided samples of ZLI 1165 and *d*-2-phenylbutanoic acid. We thank the CNR (Roma) for financial support.

(20) Ciocca, C.; Semproni, A. *Ann. Chim. Appl.* **1935**, *25*, 319-323.

(21) Birtwistle, J. S.; Lee, K.; Morrison, J. D.; Sanderson, W. A.; Mosher, H. S. *J. Org. Chem.* **1964**, *29*, 37-40.

Reversible Wavelength Shifts of Chlorophyll Induced by a Point Charge

R. C. Davis, S. L. Ditson, A. F. Fentiman, and R. M. Pearlstein*

Contribution from the Battelle Memorial Institute, Columbus Laboratories, Columbus, Ohio 43201. *Received April 27, 1981*

Abstract: The recently supported point-charge hypothesis of shifts in the optical spectra of the retinal Schiff base in rhodopsin suggests a mechanism for the anomalous red shifts of chlorophyll (Chl) spectra in vivo. This idea is tested here by synthesis of a Chl model compound, 3-demethyl-3-(aminomethyl) Chl *a*, in which a point charge is reversibly induced on the periphery of the Chl macrocycle. Chl(3a-NH_2) is formed from Chl *b* by reductive amination of the formyl group with sodium cyanoborohydride. The structure is confirmed by the Chl *a*-like absorption spectrum (λ_{max} = 661 nm, $\epsilon = 5.67 \times 10^4$ M^{-1} cm^{-1} in $CHCl_3$), by ^1H NMR, and by reversible changes in both absorption and ^1H NMR on adjustment of pH (amine nitrogen pK_a = 7.9). Chl(3a-NH_3^+) displays a reversible blue shift in its red absorption maximum of 4 nm (90 cm^{-1}) relative to Chl(3a-NH_2). Presumably, a negative charge in the same position would give a red shift of the same size; charges located differently on the macrocycle perimeter might give shifts of larger magnitude. Because such charges could be provided by polar amino acids of the Chl-binding proteins in vivo, our results lend support to a point-charge hypothesis of Chl spectral shifts.

The longest wavelength visible (or near-IR) absorbance maxima of virtually all chemical forms of chlorophyll (Chl) or bacteriochlorophyll (Bchl) found in vivo are red shifted relative to corresponding (unaggregated) forms in vitro.[1] These shifts can be as small as 225 cm^{-1} for Chl *a* in the green plant light-harvesting protein complex designated CP-II,[2] or as large as 2740 cm^{-1} for Bchl *b* in the photosynthetic bacterium, *Rps. viridis*.[3] Most of the shift is anomalous: It cannot be attributed to interactions of inter-Chl electronic transition moments (exciton interactions), or to effects analogous to changes of solvent polarity. The first point is most clearly demonstrated by a small Bchl-protein complex, analysis of the spectra of which shows that *none* of the more than 1300-cm^{-1} shift is attributable to exciton effects.[4,5] The second point is best attested by the fact that extremes of solvent polarity cause shifts of no more than 15% of those observed for Bchl *a* in vivo.[3,6,7] It has been proposed that some of the shift can be attributed to inter-Chl charge-transfer interactions,[8] but there is at present no experimental support for this hypothesis.

Recently, in the case of rhodopsin there has been considerable support for a model in which spectral shifts (red or blue) are

(1) Sauer, K. *Acc. Chem. Res.* **1978**, *11*, 257-64.
(2) Shepanski, J. F.; Knox, R. S. *Isr. J. Chem.*, in press.
(3) Thornber, J. P.; Trosper, T. L.; Strouse, C. E. "The Photosynthetic Bacteria", Clayton, R. K., Sistrom, W. R., Eds.; Plenum Press: New York, 1978; pp 133-60.
(4) (a) Bolt, J.; Sauer, K. *Biochim. Biophys. Acta* **1979**, *546*, 54-63. (b) Rafferty, C. N.; Bolt, J.; Sauer, K.; Clayton, R. K. *Proc. Natl. Acad. Sci. U.S.A.* **1979**, *76*, 4429-32.
(5) Davis, R. C.; Pearlstein, R. M. *Nature (London)* **1979**, *280*, 413-5.
(6) Sauer, K.; Lindsay Smith, J. R.; Schultz, A. J. *J. Am. Chem. Soc.* **1966**, *88*, 2681-8.
(7) Goedheer, J. C. "The Chlorophylls", Vernon, L. P., Seely, G. R., Eds.; Academic Press: New York, 1966; pp 147-84.
(8) Warshel, A. J. *J. Am. Chem. Soc.* **1979**, *101*, 744-6.

0002-7863/81/1503-6823$01.25/0